

Crystal structure of aminopentamide hydrogen sulfate, (C₁₉H₂₅N₂O)(HSO₄)James A. Kaduk ^{1,2,a)} Amy M. Gindhart ³ Stacy Gates-Rector ³ and Thomas N. Blanton ³¹Illinois Institute of Technology, 3101 S. Dearborn St., Chicago, IL 60616, USA²North Central College, 131 S. Loomis St., Naperville, IL 60540, USA³ICDD, 12 Campus Blvd., Newtown Square, PA 19073-3273, USA

(Received 27 June 2022; accepted 21 August 2022)

The crystal structure of aminopentamide hydrogen sulfate has been solved and refined using synchrotron X-ray powder diffraction data, and optimized using density functional techniques. Aminopentamide hydrogen sulfate crystallizes in space group $P2_1/c$ (#14) with $a = 17.62255(14)$, $b = 6.35534(4)$, $c = 17.82499(10)$ Å, $\beta = 96.4005(6)^\circ$, $V = 1983.906(14)$ Å³, and $Z = 4$. The structure consists of layers parallel to the bc -plane with hydrogen sulfate anions at the core and aminopentamide cations on the outside. There is a strong charge-assisted O49–H53...O52 hydrogen bond between the hydrogen sulfate anions. This hydrogen bond links the anions in a chain parallel to the b -axis. The cation forms a discrete N–H...O hydrogen bond to the anion. The amide group also forms two weaker discrete hydrogen bonds to the anion. The three N–H...O hydrogen bonds link the cations and anions into columns parallel to the b -axis. This commercial material from USP contained an unidentified impurity, the powder pattern of which could be indexed on a monoclinic unit cell. The powder pattern has been submitted to ICDD for inclusion in the Powder Diffraction File™ (PDF®). © The Author(s), 2022. Published by Cambridge University Press on behalf of International Centre for Diffraction Data. This is an Open Access article, distributed under the terms of the Creative Commons Attribution licence (<http://creativecommons.org/licenses/by/4.0/>), which permits unrestricted re-use, distribution and reproduction, provided the original article is properly cited. [doi:10.1017/S0885715622000343]

Key words: aminopentamide, Centrine[®], powder diffraction, Rietveld refinement, density functional theory

I. INTRODUCTION

“Aminopentamide sulfate” (sold under the brand name Centrine[®]) is used to control vomiting, diarrhea, and gastrointestinal (GI) pain or spasms in dogs and cats. The observed antispasmodic properties of aminopentamide hydrogen sulfate can help control the discomfort associated with anorectal disease. The systematic name (CAS Registry Number 20701-77-3) is 4-(dimethylammonium)-2,2-diphenylpentanamide hydrogen sulfate. A two-dimensional molecular diagram is shown in Figure 1.

The synthesis of aminopentamide was claimed in US Patent 2,647,926 (Speeter, 1953; Bristol Laboratories). The use of aminopentamide hydrogen sulfate in an anesthetic compound was claimed in US Patent 3,896,221 (Christie and Buckwalter, 1975; Bristol-Myers). The pharmacological activity of Centrine was reported in Hoekstra *et al.* (1954). We are unaware of any published powder diffraction data on aminopentamide hydrogen sulfate.

This work was carried out as part of a project (Kaduk *et al.*, 2014) to determine the crystal structures of large-volume commercial pharmaceuticals and include high-quality powder diffraction data for them in the Powder Diffraction File (Gates-Rector and Blanton, 2019).

II. EXPERIMENTAL

Aminopentamide hydrogen sulfate was a commercial reagent, purchased from USP (Batch #F1B273), and was used as-received. The white powder was packed into a 1.5 mm diameter Kapton capillary and rotated during the measurement at ~50 Hz. The powder pattern was measured at 295 K at beamline 11-BM (Antao *et al.*, 2008; Lee *et al.*, 2008; Wang *et al.*, 2008) of the Advanced Photon Source at Argonne National Laboratory using a wavelength of 0.458208(2) Å from 0.5 to 50° 2θ with a step size of 0.001° and a counting time of 0.1 s per step. The high-resolution powder diffraction data were collected using twelve silicon

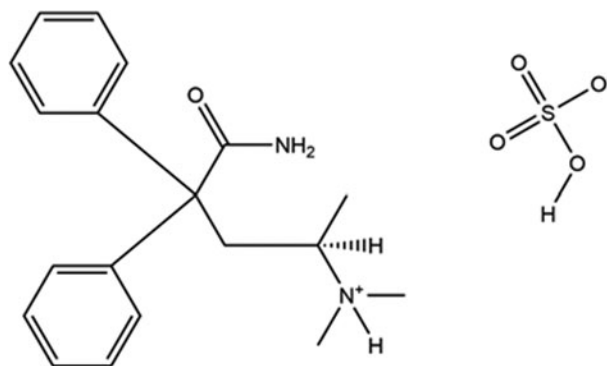


Figure 1. The 2D molecular structure of aminopentamide hydrogen sulfate.

^{a)} Author to whom correspondence should be addressed. Electronic mail: kaduk@polycrystallography.com

crystal analyzers that allow for high angular resolution, high precision, and accurate peak positions. A silicon (NIST SRM 640c) and alumina (SRM 676a) standard (ratio Al₂O₃:Si = 2:1 by weight) was used to calibrate the instrument and refine the monochromatic wavelength used in the experiment.

The pattern was difficult to index, until we allowed the possibility of up to 3 unindexed lines among the 20 peaks ($I_{\text{rel}} > 1\%$) using DICVOL14 (Louër and Boulif, 2014). A primitive monoclinic cell with $a = 17.7176$, $b = 6.3740$, $c = 17.9396$ Å, $\beta = 96.537^\circ$, $V = 2012.77$ Å³, and $Z = 4$ was obtained, with figures of merit $M(18)$ (de Wolff, 1968) and $F(18)$ (Smith and Snyder, 1979) = 20.7 and 178.6. A reduced cell search in the Cambridge Structural Database (Groom *et al.*, 2016) yielded five hits, but no structures of aminopentamide derivatives. Neither a name search on “aminopentamide” in the PDF-4 Organics database, nor a traditional search/match on the powder pattern yielded any hits.

An aminopentamide molecule was downloaded as Conformer3D_CID_22565.sdf from PubChem (Kim *et al.*, 2019). The file was converted to a *.mol2 file using Mercury (Macrae *et al.*, 2020) and to a Fenske-Hall Z-matrix using OpenBabel (O’Boyle *et al.*, 2011). The structure was solved using Monte Carlo simulated annealing (parallel tempering) techniques as implemented in FOX (Favre-Nicolin and Černý, 2002), with $(\sin\theta/\lambda)_{\text{max}} = 0.3$ Å⁻¹. The suggested space group was $P2_1/c$, which was confirmed by successful solution and refinement of the structure. Analysis of potential hydrogen bonding interactions indicated that N2 was protonated (N2...O50 = 2.612 Å), so H47 was added to it. The O49...O52 distance of 2.876 Å indicated that a proton was between these two atoms, so for the refinement H53 was placed at the midpoint of this interatomic vector. Twenty-two “extra” peaks could be indexed by DICVOL14 on a primitive monoclinic cell with $a = 17.7067$, $b = 4.1812$, $c = 38.2550$ Å, $\beta = 94.907^\circ$, and $V = 2821.82$ Å³. This phase was added to the refinement as a second Le Bail

phase. This Le Bail phase accounts for the non-overlapped impurity peaks, but has the potential to distort the intensities of the major phase in regions where there is peak overlap. Without a structure model or a pure sample of this phase, its concentration cannot be quantified without the addition of an internal standard.

Rietveld refinement was carried out using GSAS-II (Toby and Von Dreele, 2013). Only the 1.4–25.0° portion of the pattern was included in the refinement ($d_{\text{min}} = 1.058$ Å). The region 1.60–1.95° 2θ , which contains scatter from the Kapton capillary, was excluded. All non-H bond distances and angles were subjected to restraints, based on a Mercury/Mogul Geometry Check (Bruno *et al.*, 2004; Sykes *et al.*, 2011). The Mogul average and standard deviation for each quantity were used as the restraint parameters. The restraints contributed 1.8% to the final χ^2 . The hydrogen atoms were included in calculated positions, which were recalculated during the refinement using Materials Studio (Dassault Systèmes, 2021). The U_{iso} of the heavy atoms were grouped by chemical similarity. The U_{iso} for the H atoms were fixed at 1.3× the U_{iso} of the heavy atoms to which they are attached. The peak profiles were described using the generalized microstrain model. The background was modeled using a 6-term shifted Chebyshev polynomial, and a peak at 6.06° 2θ to model the scattering from the Kapton capillary and any amorphous component.

The final refinement of 110 variables using 23 279 observations and 75 restraints yielded the residuals $R_{\text{wp}} = 0.1161$ and $\text{GOF} = 2.02$. The largest peak (at S48) and hole (1.37 Å from H44) in the difference Fourier map were 0.30(7) and $-0.31(7) e\text{Å}^{-3}$, respectively. The largest errors in the difference plot (Figure 2) are in the shapes and intensities of some of the strong low-angle peaks.

The crystal structure was optimized using VASP (Kresse and Furthmüller, 1996) (fixed experimental unit cell) through the MedeA graphical interface (Materials Design, 2016). The

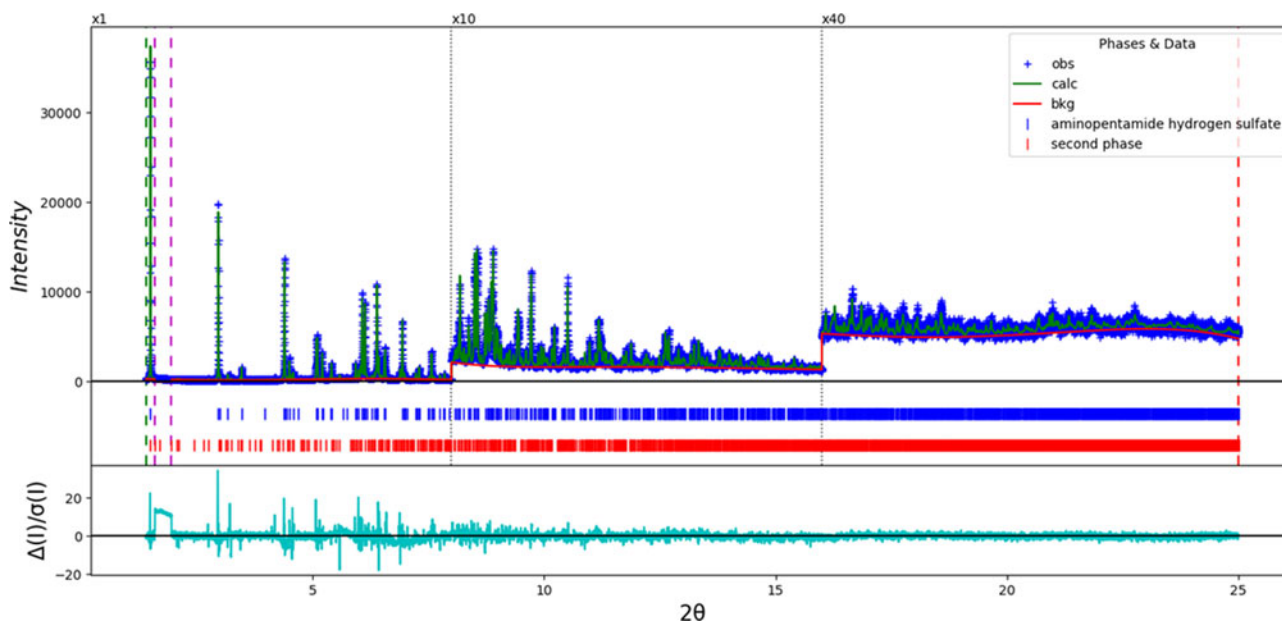


Figure 2. The Rietveld plot for the refinement of aminopentamide hydrogen sulfate. The blue crosses represent the observed data points, and the green line is the calculated pattern. The cyan curve is the normalized error plot. The vertical scale has been multiplied by a factor of 10× for $2\theta > 8.0^\circ$ and by 40× for $2\theta > 16.0^\circ$. The row of blue tick marks indicates the calculated reflection positions of aminopentamide hydrogen sulfate, and the row of red tick marks indicates the peaks from the second unidentified phase.

calculation was carried out on 16 2.4 GHz processors (each with 4 GB RAM) of a 64-processor HP Proliant DL580 Generation 7 Linux cluster at North Central College. The calculation used the GGA-PBE functional, a plane wave cutoff energy of 400.0 eV, and a k -point spacing of 0.5 \AA^{-1} leading to a $1 \times 2 \times 1$ mesh, and took ~ 42 h. A single-point density functional calculation (fixed experimental cell) and population analysis were carried out using CRYSTAL17 (Dovesi *et al.*, 2018). The basis sets for the H, C, N, and O atoms in the calculation were those of Gatti *et al.* (1994), and that for S was that of Peintinger *et al.* (2013). The calculations were run on a 3.5 GHz PC using 8 k -points and the B3LYP functional, and took ~ 3.3 h.

III. RESULTS AND DISCUSSION

The root-mean-square Cartesian displacement between the Rietveld-refined and DFT-optimized structures of the aminopentamide cation is 0.361 \AA (Figure 3); the maximum difference is 0.769 \AA at the methyl group C16. The agreement is at the upper end of the range of correct structures (van de Streek and Neumann, 2014). The agreement of the absolute positions of the cations and anions in the unit cell is reasonable (Figure 4). This discussion concentrates on the DFT-optimized structure. The asymmetric unit (with atom numbering) is illustrated in Figure 5. The best view of the crystal structure is down the b -axis (Figure 6). The structure consists of layers parallel to the bc -plane with hydrogen sulfate anions at the core and aminopentamide cations on the outside. The interlayer regions consist of parallel and herringbone stacking of phenyl rings.

All of the bond distances and angles fall within the normal ranges indicated by a Mercury/Mogul Geometry check (Macrae *et al.*, 2020). The torsion angle C9–C4–C5–C6 is flagged as unusual; this lies on the tail of a major *gauche* population of similar torsion angles. The unusual O1–C9–C4–C7 and C7–C4–C9–N3 torsion angles lie in a broad distribution of a small number of similar torsion angles. The C10–C6–C5–C4 torsion angle lies in a minor *gauche* population of mainly *trans* torsion angles. The conformation of the cation is slightly unusual.

Quantum chemical geometry optimization of the aminopentamide cation (DFT/B3LYP/6-31G*/water) using

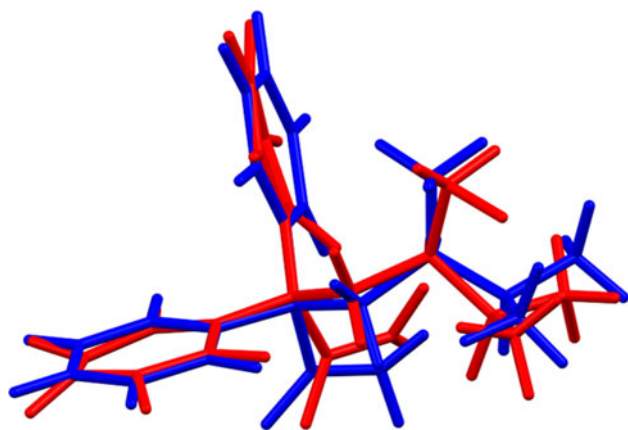


Figure 3. Comparison of the Rietveld-refined (red) and VASP-optimized (blue) structures of the aminopentamide cation. The rms Cartesian displacement is 0.361 \AA . Image generated using Mercury (Macrae *et al.*, 2020).

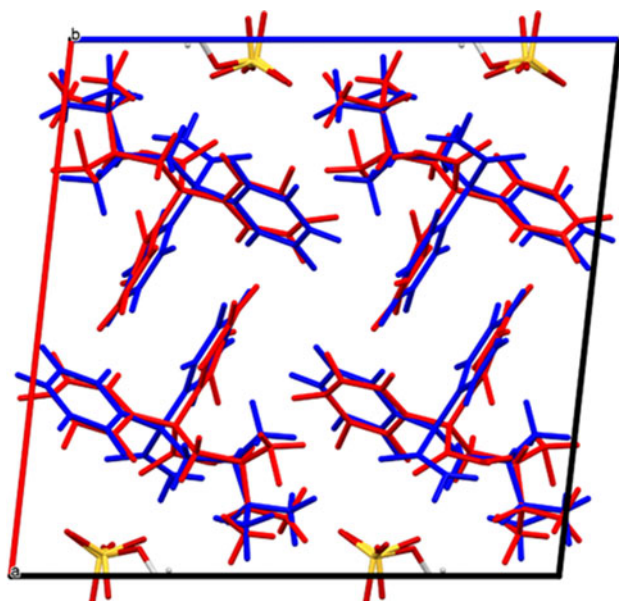


Figure 4. Comparison of the Rietveld-refined (red) and VASP-optimized (blue) structures of aminopentamide hydrogen sulfate. The cations are colored red and blue, while the hydrogen sulfate anions are colored by atom type for both structures.

Spartan '18 (Wavefunction, Inc., 2020) indicated that the observed conformation is $10.2 \text{ kcal mol}^{-1}$ higher in energy than the local minimum (Figure 7). A conformational analysis (MMFF force field) indicates that the minimum-energy conformation is $7.2 \text{ kcal mol}^{-1}$ lower in energy; the conformational differences are spread throughout the cation (Figure 8). Intermolecular interactions thus affect the solid-state conformation.

Analysis of the contributions to the total crystal energy of the structure using the Forcite module of Materials Studio (Dassault Systèmes, 2021) suggests that the intramolecular deformation energy is dominated by angle deformation

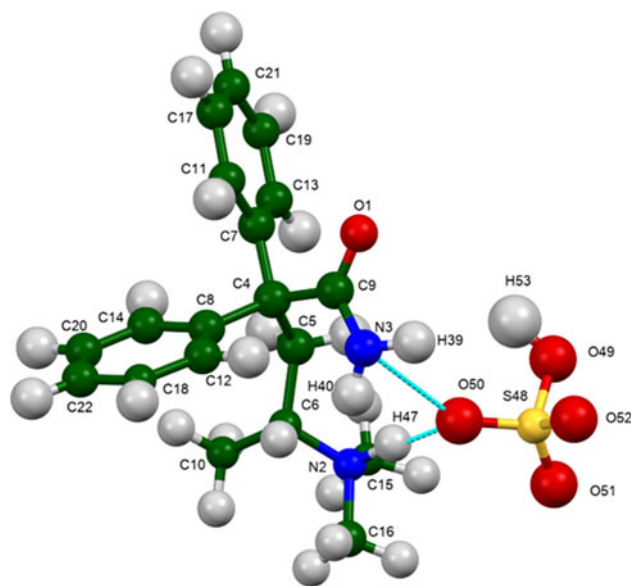


Figure 5. The asymmetric unit of aminopentamide hydrogen sulfate, with the atom numbering. The atoms are represented by 50% probability spheroids/ellipsoids. Image generated using Mercury (Macrae *et al.*, 2020).

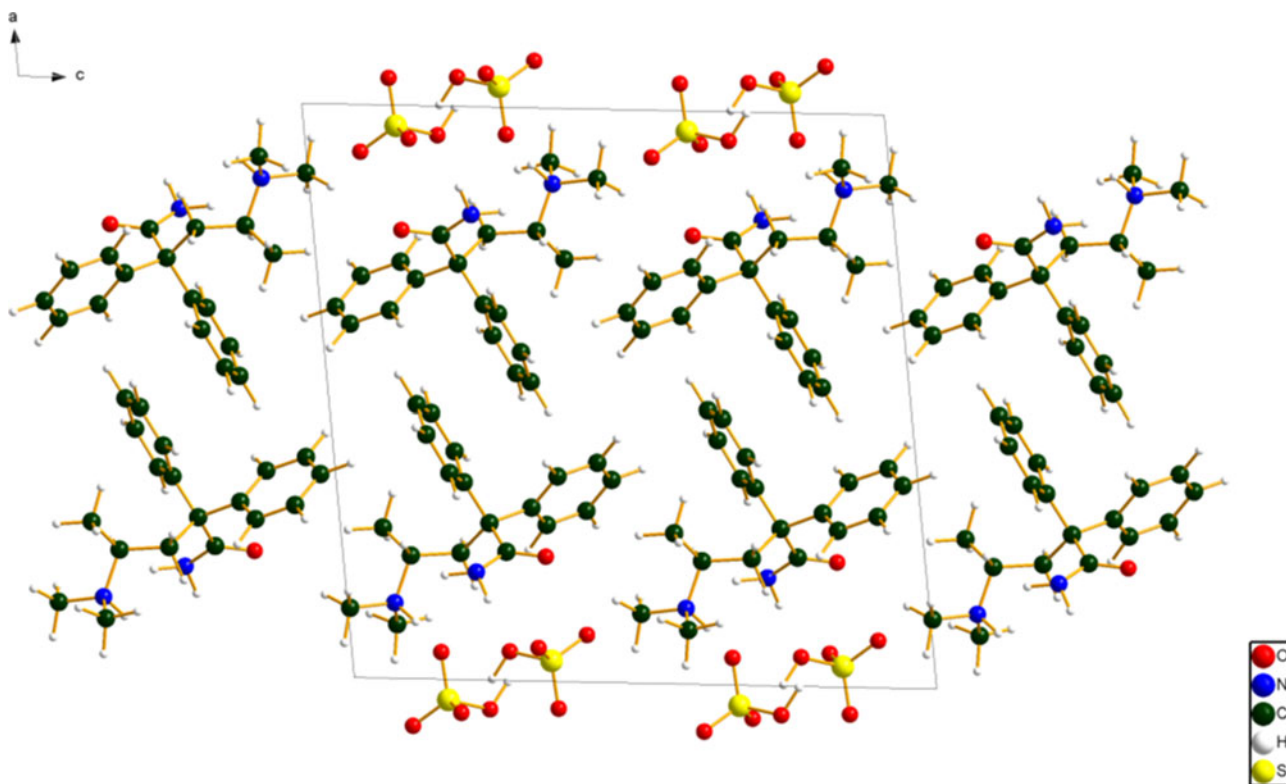


Figure 6. The crystal structure of aminopentamide hydrogen sulfate, viewed down the b -axis. Image generated using diamond (Crystal Impact, 2022).

terms. The intermolecular energy is dominated by electrostatic attractions, which in this force field analysis also include hydrogen bonds. The hydrogen bonds are better analyzed using the results of the DFT calculation.

Hydrogen bonds are prominent in the structure (Table I). There is a strong charge-assisted O49–H53...O52 hydrogen bond between the hydrogen sulfate anions. The energy of this hydrogen bond was calculated using the correlation of Rammohan and Kaduk (2018). This hydrogen bond links the anions parallel to the b -axis in a chain with a graph set

(Etter, 1990; Bernstein *et al.*, 1995; Shields *et al.*, 2000) $C1, I(4)$. There is also a weaker O49–H53...S48 interaction. The cation forms a discrete N2–H47...O50 hydrogen bond to the anion. The energies of the N–H...O hydrogen bonds were calculated using the correlation of Wheatley and Kaduk (2019). The amide group N3/H39/H40 also forms two weaker discrete hydrogen bonds to the anion. The three N–H...O hydrogen bonds link the cations and anions into columns parallel to the b -axis. There are three C–H...O hydrogen bonds, both to the anion and to the carbonyl oxygen O1. The

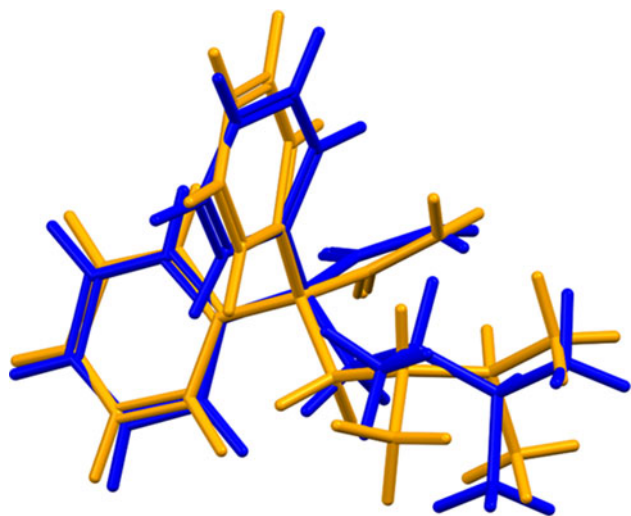


Figure 7. Comparison of the VASP-optimized (blue) and local minimum-energy conformations (orange) of the aminopentamide cation.

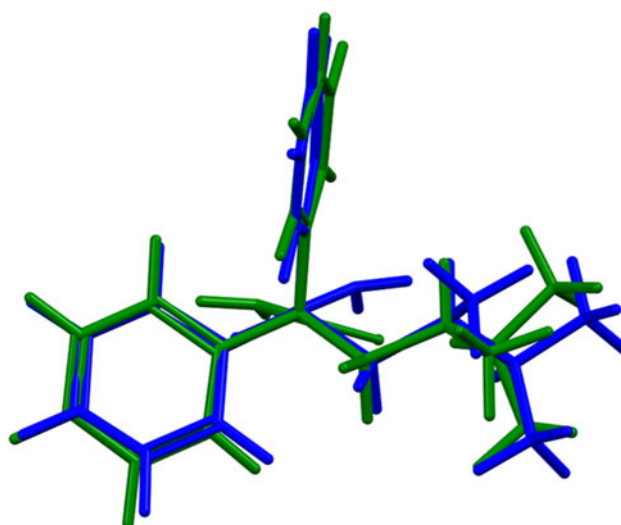


Figure 8. Comparison of the VASP-optimized (blue) and global minimum-energy conformations (green) of the aminopentamide cation.

TABLE I. Hydrogen bonds (CRYSTAL17) in aminopentamide hydrogen sulfate.

H-Bond	D-H (Å)	H...A (Å)	D...A (Å)	D-H...A (°)	Overlap (<i>e</i>)	<i>E</i> (kcal mol ⁻¹)
O49–H53...O52	1.041	1.530	2.557	167.8	0.090	16.4
O49–H53...S48	1.041	2.241	3.299	134.9	0.012	
N2–H47...O50	1.067	1.600	2.662	172.5	0.085	6.7
N3–H39...O49	1.029	1.935	2.964	177.8	0.040	4.6
N3–H40...O50	1.014	2.450	2.844	102.3	0.009	2.2
C5–H23...O52	1.102	2.726	3.770	158.0	0.013	
C15–H33...O51	1.096	2.603	3.595	150.2	0.014	
C16–H37...O1	1.096	2.647	3.689	158.6	0.012	
C10–H28...C14	1.096	2.440 ^a	3.339	138.4	0.013	
C21–H45...C18	1.089	2.460	3.473	151.2	0.010	

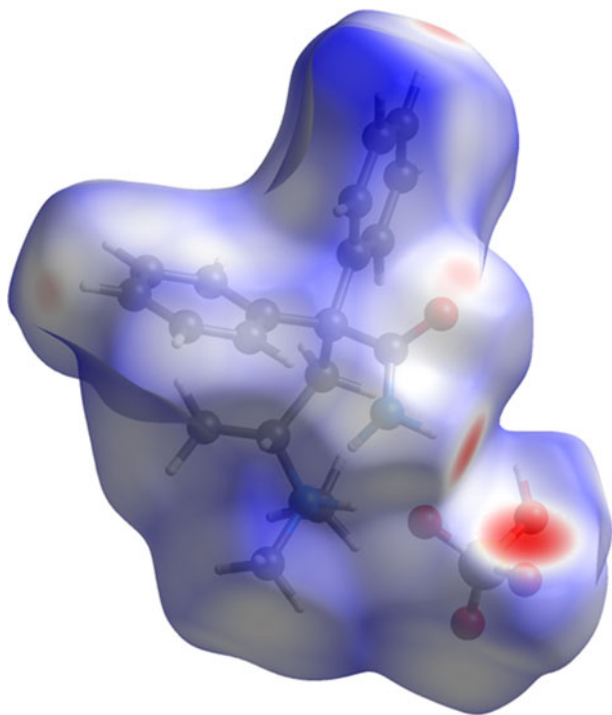
^aIntramolecular.

Figure 9. The Hirshfeld surface of aminopentamide hydrogen sulfate. Intermolecular contacts longer than the sums of the van der Waals radii are colored blue, and contacts shorter than the sums of the radii are colored red. Contacts equal to the sums of radii are white.

intramolecular C10–H28...C14 hydrogen bond links a methyl group and a phenyl ring. The C21–H45...C18 hydrogen bonds indicate an end-side phenyl–phenyl ring interaction.

The volume enclosed by the Hirshfeld surface of aminopentamide hydrogen sulfate (Figure 9; Hirshfeld, 1977; Turner *et al.*, 2017) is 487.96 Å³, 98.38% of 1/4 the unit cell volume. The packing density is thus fairly typical. The only significant close contacts (red in Figure 9) involve the hydrogen bonds. The average volume/non-hydrogen atom is 18.4 Å³.

The Bravais–Friedel–Donnay–Harker (Bravais, 1866; Friedel, 1907; Donnay and Harker, 1937) morphology suggests that we might expect platy morphology for aminopentamide hydrogen sulfate, with {100} as the major faces. A second-order spherical harmonic model was included in the refinement. The texture index was 1.014(0), indicating that preferred orientation was slight in this rotated capillary

specimen. The powder pattern of aminopentamide hydrogen sulfate from this synchrotron data set has been submitted to ICDD for inclusion in the Powder Diffraction File.

IV. DEPOSITED DATA

The Crystallographic Information Framework (CIF) files containing the results of the Rietveld refinement (including the raw data) and the DFT geometry optimization were deposited with the ICDD. The data can be requested at info@icdd.com.

ACKNOWLEDGEMENTS

The use of the Advanced Photon Source at Argonne National Laboratory was supported by the U.S. Department of Energy, Office of Science, Office of Basic Energy Sciences, under Contract No. DE-AC02-06CH11357. This work was partially supported by the International Centre for Diffraction Data. We thank Lynn Ribaud and Saul Lapidus for their assistance in the data collection.

CONFLICT OF INTEREST

The authors have no conflicts of interest to declare.

- Antao, S. M., Hassan, I., Wang, J., Lee, P. L., and Toby, B. H. (2008). "State-of-the-art high-resolution powder X-ray diffraction (HRPXRD) illustrated with Rietveld refinement of quartz, sodalite, tremolite, and meionite," *Can. Mineral.* **46**, 1501–1509.
- Bernstein, J., Davis, R. E., Shimon, L., and Chang, N. L. (1995). "Patterns in hydrogen bonding: functionality and graph set analysis in crystals," *Angew. Chem., Int. Ed. Engl.* **34**(15), 1555–1573.
- Bravais, A. (1866). *Études Cristallographiques* (Gauthier Villars, Paris).
- Bruno, I. J., Cole, J. C., Kessler, M., Luo, J., Motherwell, W. D. S., Purkis, L. H., Smith, B. R., Taylor, R., Cooper, R. I., Harris, S. E., and Orpen, A. G. (2004). "Retrieval of crystallographically-derived molecular geometry information," *J. Chem. Inf. Comput. Sci.* **44**, 2133–2144.
- Christie, G. J. and Buckwalter, F. H. (1975). "Anesthetic compositions," U.S. Patent 3,896,221.
- Crystal Impact - Dr. H. Putz & Dr. K. Brandenburg. (2022). *Diamond - Crystal and Molecular Structure Visualization*. Kreuzherrenstr. 102, 53227 Bonn, Germany. Available at: <https://www.crystalimpact.de/diamond>.
- Dassault Systèmes (2021). *Materials Studio 2021* (BIOVIA, San Diego, CA).
- de Wolff, P. M. (1968). "A simplified criterion for the reliability of a powder pattern indexing," *J. Appl. Crystallogr.* **1**, 108–113.
- Donnay, J. D. H. and Harker, D. (1937). "A new law of crystal morphology extending the law of Bravais," *Am. Mineral.* **22**, 446–447.

- Dovesi, R., Erba, A., Orlando, R., Zicovich-Wilson, C. M., Civalleri, B., Maschio, L., Rerat, M., Casassa, S., Baima, S., Salustro, J., and Kirtman, B. (2018). "Quantum-mechanical condensed matter simulations with CRYSTAL," *WIREs Comput. Mol. Sci.* **8**, e1360.
- Etter, M. C. (1990). "Encoding and decoding hydrogen-bond patterns of organic compounds," *Acc. Chem. Res.* **23**(4), 120–126.
- Favre-Nicolin, V. and Černý, R. (2002). "FOX, "free objects for crystallography: a modular approach to ab initio structure determination from powder diffraction," *J. Appl. Crystallogr.* **35**, 734–743.
- Friedel, G. (1907). "Etudes sur la loi de Bravais," *Bull. Soc. Fr. Mineral.* **30**, 326–455.
- Gates-Rector, S. and Blanton, T. (2019). "The Powder Diffraction File: a quality materials characterization database," *Powder Diffr.* **39**(4), 352–360.
- Gatti, C., Saunders, V. R., and Roetti, C. (1994). "Crystal-field effects on the topological properties of the electron-density in molecular crystals - the case of urea," *J. Chem. Phys.* **101**, 10686–10696.
- Groom, C. R., Bruno, I. J., Lightfoot, M. P., and Ward, S. C. (2016). "The Cambridge Structural Database," *Acta Crystallogr., Sect. B: Struct. Sci., Cryst. Eng. Mater.* **72**, 171–179.
- Hirshfeld, F. L. (1977). "Bonded-atom fragments for describing molecular charge densities," *Theor. Chim. Acta* **44**, 129–138.
- Hoekstra, J. B., Tisch, D. E., Rakićen, N., and Dickison, H. L. (1954). "The pharmacological activity of *dl*-alpha, alpha-diheny, gamma-dimethylaminovaleramide (Centrine)," *J. Pharmacol. Exp. Ther.* **110**, 55–67.
- Kaduk, J. A., Crowder, C. E., Zhong, K., Fawcett, T. G., and Suchomel, M. R. (2014). "Crystal structure of atomoxetine hydrochloride (Strattera), C₁₇H₂₂NOCl," *Powder Diffr.* **29**(3), 269–273.
- Kim, S., Chen, J., Cheng, T., Gindulyte, A., He, J., He, S., Li, Q., Shoemaker, B. A., Thiessen, P. A., Yu, B., Zaslavsky, L., Zhang, J., and Bolton, E. E. (2019). "PubChem 2019 update: improved access to chemical data," *Nucleic Acids Res.* **47**(D1), D1102–D1109. doi:10.1093/nar/gky1033.
- Kresse, G. and Furthmüller, J. (1996). "Efficiency of ab-initio total energy calculations for metals and semiconductors using a plane-wave basis set," *Comput. Mater. Sci.* **6**, 15–50.
- Lee, P. L., Shu, D., Ramanathan, M., Preissner, C., Wang, J., Beno, M. A., Von Dreele, R. B., Ribaud, L., Kurtz, C., Antao, S. M., Jiao, X., and Toby, B. H. (2008). "A twelve-analyzer detector system for high-resolution powder diffraction," *J. Synchrotron Radiat.* **15**(5), 427–432.
- Louër, D. and Boulton, A. (2014). "Some further considerations in powder diffraction pattern indexing with the dichotomy method," *Powder Diffr.* **29**, S7–S12.
- Macrae, C. F., Sovago, I., Cottrell, S. J., Galek, P. T. A., McCabe, P., Pidcock, E., Platings, M., Shields, G. P., Stevens, J. S., Towler, M., and Wood, P. A. (2020). "Mercury 4.0: from visualization to design and prediction," *J. Appl. Crystallogr.* **53**, 226–235.
- Materials Design (2016). *Medea 2.20.4* (Materials Design Inc., Angel Fire, NM).
- O'Boyle, N., Banck, M., James, C. A., Morley, C., Vandermeersch, T., and Hutchison, G. R. (2011). "Open babel: an open chemical toolbox," *J. Cheminf.* **3**, 33. doi:10.1186/1758-2946-3-33.
- Peintinger, M. F., Vilela Oliveira, D., and Bredow, T. (2013). "Consistent Gaussian basis sets of triple-zeta valence with polarization quality for solid-state calculations," *J. Comput. Chem.* **34**, 451–459.
- Rammohan, A. and Kaduk, J. A. (2018). "Crystal structures of alkali metal (group 1) citrate salts," *Acta Crystallogr., Sect. B: Struct. Sci., Cryst. Eng. Mater.* **74**, 239–252. doi:10.1107/S2052520618002330.
- Shields, G. P., Raithby, P. R., Allen, F. H., and Motherwell, W. S. (2000). "The assignment and validation of metal oxidation states in the Cambridge Structural Database," *Acta Crystallogr., Sect. B: Struct. Sci., Cryst. Eng. Mater.* **56**(3), 455–465.
- Smith, G. S. and Snyder, R. L. (1979). "A criterion for rating powder diffraction patterns and evaluating the reliability of powder-pattern indexing," *J. Appl. Crystallogr.* **12**, 60–65.
- Speeter, M. E. (1953). "Diphenyl-dimethyl-aminovaleramide," U.S. Patent 2,647,926.
- Sykes, R. A., McCabe, P., Allen, F. H., Battle, G. M., Bruno, I. J., and Wood, P. A. (2011). "New software for statistical analysis of Cambridge Structural Database data," *J. Appl. Crystallogr.* **44**, 882–886.
- Toby, B. H. and Von Dreele, R. B. (2013). "GSAS II: the genesis of a modern open source all purpose crystallography software package," *J. Appl. Crystallogr.* **46**, 544–549.
- Turner, M. J., McKinnon, J. J., Wolff, S. K., Grimwood, D. J., Spackman, P. R., Jayatilaka, D., and Spackman, M. A. (2017). *CrystalExplorer17* (University of Western Australia). Available at: <https://crystalexplorer.scb.uwa.edu.au>.
- van de Streek, J. and Neumann, M. A. (2014). "Validation of molecular crystal structures from powder diffraction data with dispersion-corrected density functional theory (DFT-D)," *Acta Crystallogr., Sect. B: Struct. Sci., Cryst. Eng. Mater.* **70**(6), 1020–1032.
- Wang, J., Toby, B. H., Lee, P. L., Ribaud, L., Antao, S. M., Kurtz, C., Ramanathan, M., Von Dreele, R. B., and Beno, M. A. (2008). "A dedicated powder diffraction beamline at the advanced photon source: commissioning and early operational results," *Rev. Sci. Instrum.* **79**, 085105.
- Wavefunction, Inc. (2020). Spartan '18 Version 1.4.5, Wavefunction Inc., 18401 Von Karman Ave., Suite 370, Irvine, CA 92612.
- Wheatley, A. M. and Kaduk, J. A. (2019). "Crystal structures of ammonium citrates," *Powder Diffr.* **34**, 35–43.